

AUTOMATIC SOFT PLAQUE DETECTION FROM CTA

A Thesis
Presented to
The Academic Faculty

by

Ponnappan Arumuganainar

In Partial Fulfillment
of the Requirements for the Degree
Master of Science in
Bioengineering

Department of Biomedical Engineering
Georgia Institute of Technology
August 2008

AUTOMATIC SOFT PLAQUE DETECTION FROM CTA

Approved by:

Professor Allen Tannenbaum, Advisor
Department of Biomedical Engineering
Georgia Institute of Technology

Professor Oskar Skrinjar
Department of Biomedical Engineering
Georgia Institute of Technology

Professor Anthony Yezzi
School of Electrical and Computer
Engineering
Georgia Institute of Technology

Date Approved: 8 August 2008

To my Parents, Brother and Sister

ACKNOWLEDGEMENTS

I sincerely thank my advisor Dr. Allen Tannenbaum for giving me support and guidance to carry on my research for the past two years. I take this opportunity to extend my gratitude to Dr. Anthony Yezzi and Dr. Oskar Skrinjar for teaching me various image processing techniques and for being the members of this thesis committee. I would also like to thank Drs. Arthur Stillman and Paolo Raggi of the Emory Medical School for their help in working with and understanding CTA imagery. I would like to thank the members of the Tannenbaum-Lab for their friendship and support.

TABLE OF CONTENTS

DEDICATION	iii
ACKNOWLEDGEMENTS	iv
LIST OF TABLES	vii
LIST OF FIGURES	viii
SUMMARY	x
I INTRODUCTION	1
1.1 Atherosclerosis	1
1.2 Detection of Atherosclerosis	4
1.3 Computed Tomography	4
1.4 CT - Angiography	7
1.5 Organization of Thesis	8
II SEGMENTATION OF CORONARY VESSELS	11
2.1 Vessel Filter	11
2.2 Active Contour based segmentation	14
2.2.1 Edge based active contours	14
2.2.2 Region based active contours	16
2.3 Level set technique	17
2.3.1 Explicit and implicit representations of curves	17
2.3.2 Level set representation of active contour models	18
2.4 Bayesian based active surface segmentation	20
III WATERSHED BASED DETECTION OF SOFT PLAQUE	23
3.1 Local convexity Vs Global convexity	23
3.2 Watershed transformation	24
3.3 Automatic detection of local concavity	25
3.4 Results and Discussion	27

IV	LOCAL REGION BASED SEGMENTATION	32
4.1	Segmentation issues with traditional energy schemes	32
4.1.1	Edge based energy	32
4.1.2	Region based energy	33
4.2	Local Region based energy	35
4.2.1	Examples of Local Region based Energy	35
4.2.2	Curve shortening flow for Hybrid Energy	37
4.3	Blob and Lung Correction	38
4.4	Segmentation Results	39
V	CONCLUSION	46
	REFERENCES	47

LIST OF TABLES

1	Possible patterns of the gradient	12
2	Possible patterns in 3D, based on eigenvalues from Hessian matrix. Adapted from [15].	13

LIST OF FIGURES

1	Progression of Atherosclerotic lesion (Adapted from [2])	2
2	Cardiac Ischemia. (Source: [6])	3
3	Components of CT Scanner (source: [7])	5
4	Various Generations of CT scanners. Top row: Generation 1 (on left), Generation 2 (on right). Bottom row: Generation 3 (on left), Genera- tion 4 (on right) (source: [7])	6
5	Comparison of X-ray attenuation constants of Iodine and Lead with various physiological tissues. (Source: [8])	7
6	Intensity of Soft Plaque in CTA imaging	9
7	Detection of Soft Plaque	10
8	Results of the Hessian Filter	15
9	A closed curve(Left) and its Level set representation(Right)	19
10	Results of Bayesian active contour segmentation	22
11	A 2D energy representation of catchment basins	25
12	A 3D surface representation of the energy shown in figure 11	25
13	A 2D object with concavity (Left). The distance function calculated in the region between the object boundary and the dilated and 'curvature- smoothed' object boundary (Right).	29
14	Results of identification of concavity (for object in Figure 13). This im- age shows the watershed catchment areas (Left) and the largest catch- ment area indicates the concavity in the boundary (Right).	29
15	A 2D synthetic vessel with concavity (Left). The distance function calculated in the region between the object boundary and the dilated and 'curvature-smoothed' object boundary (Right).	30
16	Results of identification of concavity (for object in Figure 15). This image shows the watershed catchment areas (Left). The largest catch- ment area indicates the concavity in the boundary (Right).	30
17	Results of identification of soft plaque deposits in coronary arteries of dataset 1. The Red color surface indicates the approximate location of the plaque.	31

18	Results of identification of soft plaque deposits in coronary arteries of dataset 2. The Red color surface indicates the approximate location of the plaque.	31
19	Soft plaque intensity in the region of overlap identified by EM algorithm [32] [33].	34
20	The exterior and interior of local neighborhood regions. The Yellow dot corresponds to $C(s)$. Red Ball corresponds to $B_r(C(s))$	36
21	Dataset1: Before and After Blob Correction	40
22	Dataset2: Before and After Blob and Lung Correction	40
23	Dataset1: A 2D Slice of the dataset	42
24	Dataset1: Initial Contour for Hybrid scheme	42
25	Dataset1: Final Contour after evolution	42
26	Dataset2: A 2D Slice of the dataset	43
27	Dataset2: Initial Contour for Hybrid scheme	43
28	Dataset2: Final Contour after evolution	43
29	Dataset1: Result of 3D Segmentation using Local Region based energy.	44
30	Dataset2: Result of 3D Segmentation using Local Region based energy.	45

SUMMARY

This thesis explores two possible ways of detecting soft plaque present in the coronary arteries, using CTA imagery. The coronary arteries are vessels that supply oxidized blood to the cardiac muscle and are thus important for the proper functioning of heart. Cholesterol or reactive oxygen species from cigarette smoke and other toxins may get adhered to the walls of coronary arteries and trigger chronic inflammation that leads to formation of the soft plaque. When the soft plaque grows bigger in volume, it occludes the blood flow to the cardiac muscle and finally results in ischemic heart attack. Moreover, smaller plaque can easily rupture due to the blood flow in arteries and can result in complications such as stroke. Hence there is a need to detect the soft plaque using non-invasive or minimally invasive techniques.

In CTA imagery, the cardiac muscle appears as a dark gray color, while the blood appears as dull white color and the calcified plaque appears as bright white. The soft plaque has an intensity which falls between the intensity level of the blood and cardiac muscle, making it difficult to directly segment the soft plaque using standard segmentation methods. Soft plaque in its advanced stages forms a concavity in the blood lumen. A watershed based segmentation method was used to detect the presence of this concavity which in turn identifies the location of the soft plaque. For segmenting the soft plaque at its earlier stages, a novel segmentation technique was used. In this technique the surface is evolved based on a region-based energy calculated in the local neighborhood around each point on the evolving surface. This method seems to be superior to the watershed based segmentation method in detecting smaller plaque deposits.

CHAPTER I

INTRODUCTION

1.1 Atherosclerosis

The heart, an organ made of cardiac muscle, is the center of the circulatory system. For the proper functioning (expansion/contraction) of the cardiac muscle, the heart has to get its own supply of oxygenated blood via the coronary arteries. A part of the oxygenated blood that is pumped out of heart (through the aorta) re-enters the heart muscle through the coronary arteries and keeps the heart functioning. Most cardiovascular emergencies are directly caused by coronary artery disease. In 2005, over 70% of cardio-vascular disease related deaths in the United States were directly related to atherosclerosis, a coronary artery disease [1]. Atherosclerosis is a degenerative inflammatory disease that results in narrowing of mostly the coronary arteries. This is caused by fatty deposits such as cholesterol (particularly Low Density Lipoprotein (LDL)), on the interior walls of the coronary arteries. As the plaque progresses the walls become too narrow or occluded. This results in the reduction of the blood flow to the heart muscle and the cardiac cells that no longer receive sufficient oxygen begin to die, resulting in heart attack. The atherosclerotic lesions are also vulnerable to rupture and the ruptured segments can block other arteries in the circulatory system resulting in complications such as stroke. In this section, we will briefly describe the progression of atherosclerosis in the coronary arteries.

This disease typically starts with an endothelial dysfunction, which may be caused by elevated levels of LDL, free radicals from cigarette smoking, diabetes, high blood pressure, genetic and microbial causes. The endothelial dysfunction leads to compensatory responses that change the normal homeostatic properties of the endothelium.

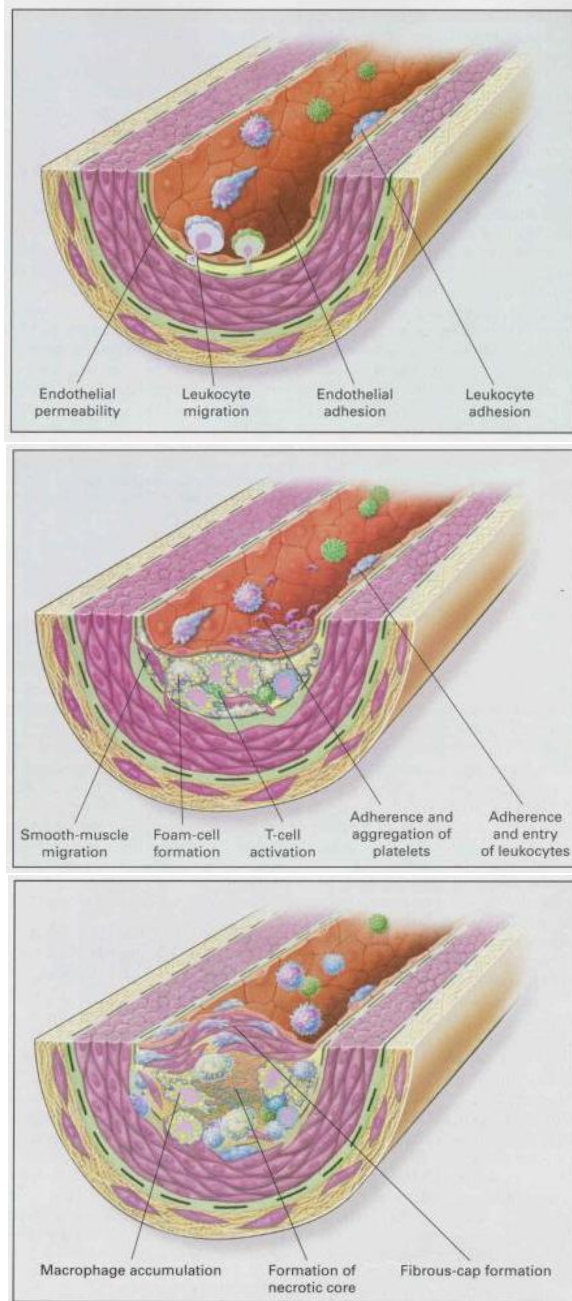


Figure 1: Progression of Atherosclerotic lesion (Adapted from [2])

The adhesiveness of anti-inflammatory cells like leukocytes and platelets with the endothelium increases. The endothelium starts to form vasoactive molecules, cytokines, and growth factors. The monocyte-derived macrophages and specific subtypes of T-lymphocytes start playing a major role in this inflammatory response [2]. Typically

this inflammatory response does not effectively neutralize or remove the dysfunction or the offending agents and continues indefinitely like a positive feedback to form an intermediate lesion. If these responses continue unabated, they start to thicken the artery wall. The progression of the atherosclerotic lesion is shown in Figure 1.

LDL is a major cause of the endothelium injury. It undergoes oxidation when it is trapped in the arteries. When the LDL is trapped by the macrophages, it forms a reactive oxygen species namely lipid peroxide, which starts accumulating to form the foam cells. These trapped LDL particles in turn increase the production of LDL receptor proteins, which in turn trap more LDL entities resulting into a cycle of inflammation that eventually results in the formation of soft plaque [2]. Recent study shows that 50% of acute coronary and myocardial infraction cases are due to the instability and the rupture of the plaque/lesions at non occlusive parts [2] [3]. When the plaque breaks the macrophages rush to the spot and start accumulating/clogging, resulting in the complete occlusion of the vessel and ischemia that results in heart attack. This is illustrated in the Figure 2.

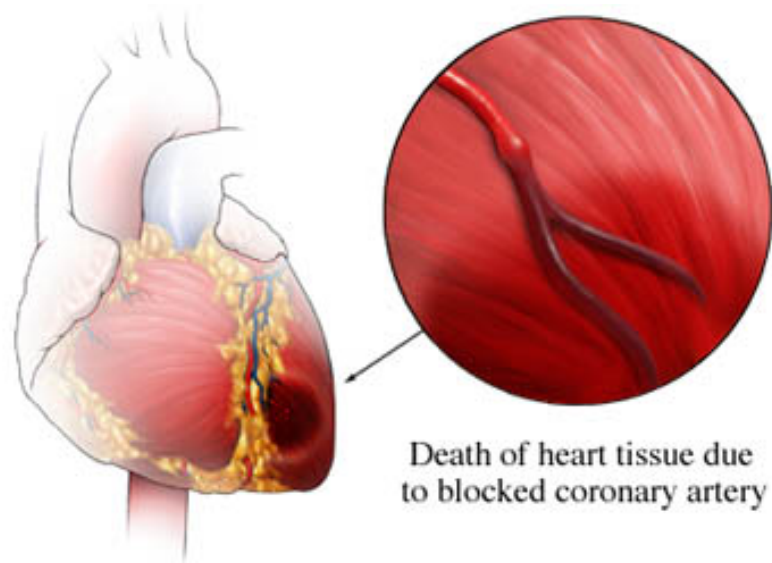


Figure 2: Cardiac Ischemia. (Source: [6])

1.2 Detection of Atherosclerosis

In the past, in order to detect the extent of the atherosclerosis, the invasive coronary angiography was used as the gold standard. This method is generally safe and less than one serious complication arises out of every thousand cases. A recent survey indicates that over 4 million cardiac catheterizations were performed yearly (before the development of non invasive imaging techniques) in the United States for the purpose of estimation of atherosclerosis. Of these, up to 27% have either healthy coronary arteries or arteries with minimal atherosclerosis [4]. Cardiac catheterization is an expensive and invasive procedure and is a much valuable resource that should be used mainly for therapeutic rather than diagnostic purposes. This impelled the development of noninvasive means for accurately detecting coronary atherosclerosis. MRI, Multi slice(MBCT) and Electron beam(EBCT) computed tomography are now being used for the diagnosis of atherosclerosis. Among these methods CT has a better spatial resolution and has been the preferred choice of cardiac radiologists.

1.3 Computed Tomography

Over the past 25 years, Computed Tomography has evolved as a powerful tool in anatomical imaging. Recent improvements in the CT technology has helped to improve the spatial and temporal resolution of CT imaging, enabling it to be used for cardiac imaging in general and coronary imaging in particular. The schematic diagram of the various components of a CT scanner are shown in Figure 3. The various generations of CT technology [5] are explained in this section.

First generation: This CT design had a single X-ray source and single X-ray detector. The source transmits a single pencil beam and the source and the detector are rigidly coupled. The beam is translated across the patient to obtain a set of parallel projection at a particular angle. Similar projections are obtained at different angles by rotating the source/ detector pair. The above measurements are used to

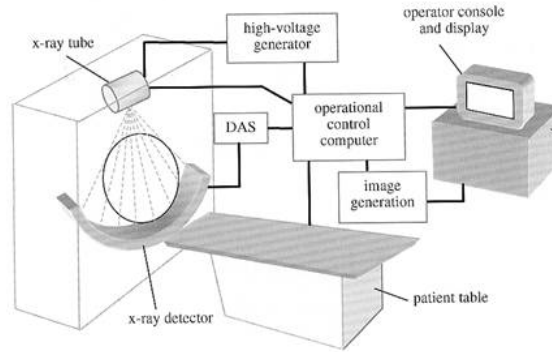


Figure 3: Components of CT Scanner (source: [7])

reconstruct a slice in 2D by using the Fourier slice theorem. Multiple slices are obtained by translating the patient and repeating the above process. This method was very slow.

Second Generation: In this design the fact that the X-ray source emits X-rays over a large angle is used. In this design there is a single X-ray source that emits a fan beam of X-rays. There are multiple number of detectors that detect the X-ray intensity at different angles with respect to the source. Multiple fan beam projections are obtained and a fan beam reconstruction algorithm is used to reconstruct the slice. The source and the detector array are translated as in the first generation system to obtain more 2D slices. This system was more efficient and faster than the first generation and reduced the amount of radiation dose received by the patient.

Third Generation: This design was a result of the improvement in the X-ray detector and data acquisition technology. It was possible to develop detectors that span over a large cross-section of the patient and with high spatial resolution. With this detector design there was no need to translate the detector array across the patient and it was only required to rotate the detector array and the X-ray source. This led to the development of helical CT machine where the patient table is moved continuously with a constant speed and the detector array and X-ray source rotate around the patient table. This design reduced the acquisition time considerably,

enabling the CT to be used for cardiac imaging.

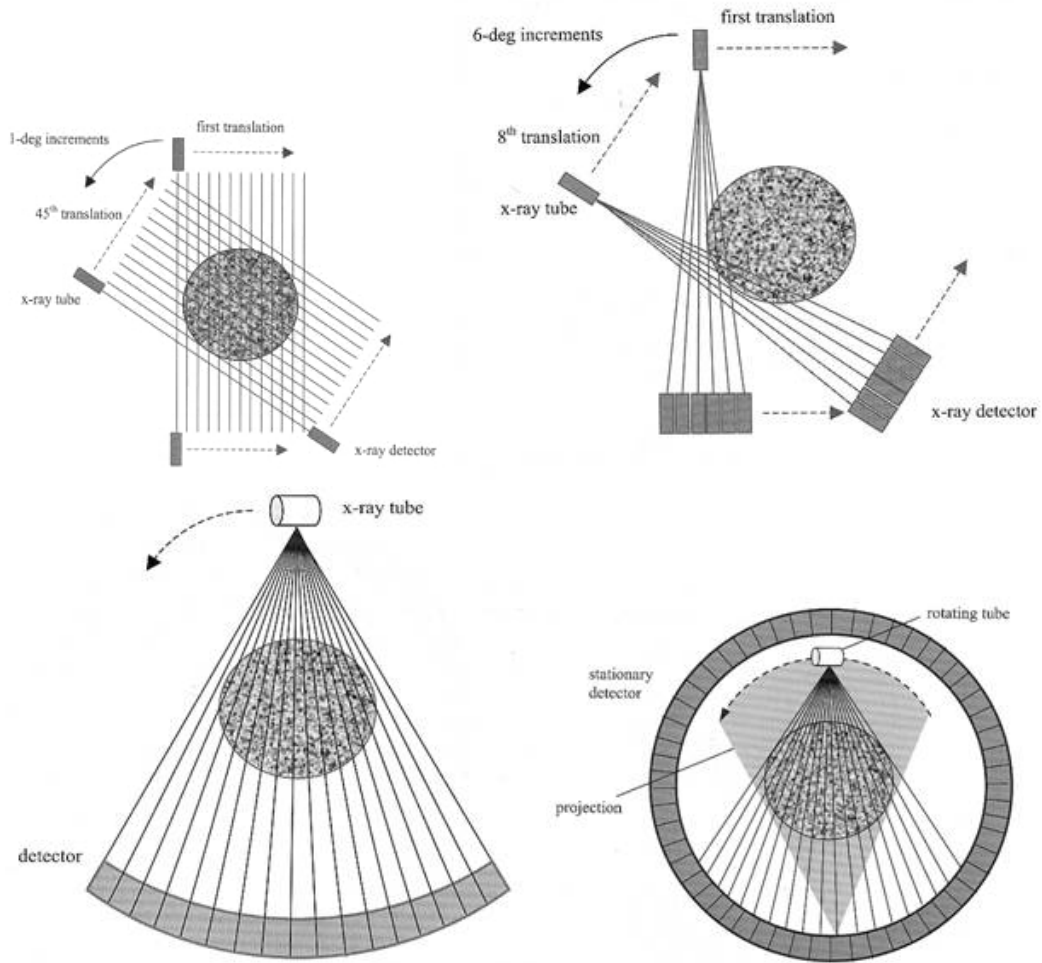


Figure 4: Various Generations of CT scanners. Top row: Generation 1 (on left), Generation 2 (on right). Bottom row: Generation 3 (on left), Generation 4 (on right) (source: [7])

Fourth Generation: This system was developed to prevent the ring artifacts common in the third generation systems. This design had a stationary detector ring and a rotating X-ray source. This resulted in a great reduction in the complexity of the system. Since the stationary detector has a larger acceptance angle, it is more sensitive to the scattered radiation. This design requires a large amount of detector cells in the stationary detector array, thereby increasing the cost of the CT scanner. As an improvement to this design, the source of X-ray beam is moved around by steering

the electron beam around the X-ray generating anode (electron beam hits the anode and produces X-rays), instead of physically moving the whole source. Since electron beam can be steered more rapidly, this improved design can attain higher acquisition rates. This design is called as Electron Beam CT.

The acquisition methods used in the various generations of the CT scanners are provided in the Figure 4.

1.4 CT - Angiography

In CT images, the bones that attenuate the X-rays to a large extent appear white in color (higher intensity value), the muscle and organs that attenuate the X-rays moderately appear as gray intensities and air/vacuum that does not attenuate the X-ray appear as black in color (low intensity value). The blood does not attenuate the X-rays as good as the bones and muscle, and hence are supposed to have intensity values ranging between gray and black.

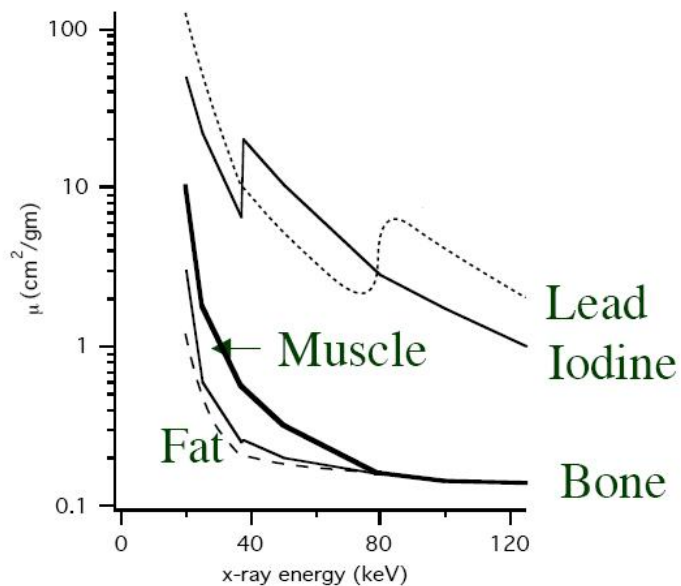


Figure 5: Comparison of X-ray attenuation constants of Iodine and Lead with various physiological tissues. (Source: [8])

In order to visualize the blood and the blood vessels using CT images, a radiocontrast agent should be injected in to the blood. The presence of radiocontrast in the blood attenuates the X-rays much better and results in higher intensity corresponding to the location of the blood. Typically radiocontrasts have an element that has a higher atomic number, so that it can efficiently attenuate the X-rays. A comparison of the attenuation constant of Iodine and Lead with various tissue types of the body are provided in Figure 5. While choosing the radiocontrast agent, care must be taken to ensure that the radiocontrast is not harmful to the patients who are being administered with it. Two examples of radiocontrast agents that can be used for enhancing the anatomical imaging by CT are as follows:

1. Barium sulphate based contrast agent. This is primarily used in the imaging of the gastro intestinal tract.
2. Iodine based contrast agent. This is used for coronary angiography studies. The agent can be either administered by an intravenous injection or by catheterization.

The intensities of the blood, cardiac muscle, air and soft plaque in the CTA images are shown in Figure 6. For our research we used anonymized CTA datasets that were provided to us by expert cardiac radiologists at Emory Medical School. These datasets had an in-plane resolution in the order of 0.4mm. The slice thickness too was in the order of 0.4mm.

1.5 Organization of Thesis

As a first step towards the detection of soft plaque, we need to segment the coronary vessels. Chapter 2 of this thesis talks about the Hessian based vessel filter and Bayesian driven level set active contours techniques that are used to extract the coronary arteries from the CTA images. Once the coronary arteries (blood lumen)

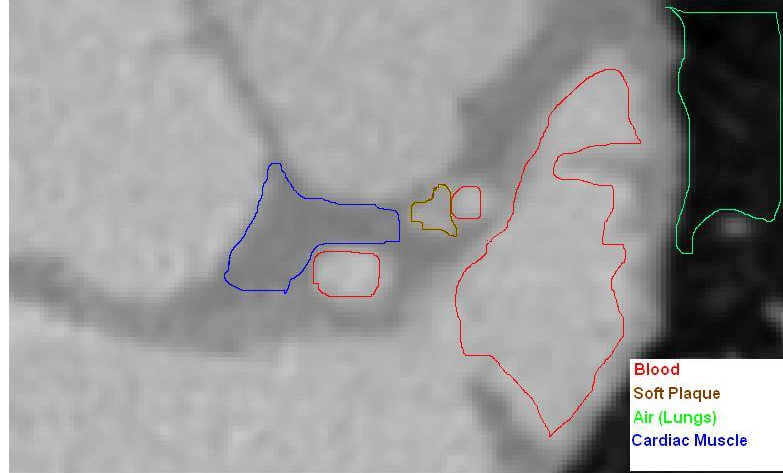


Figure 6: Intensity of Soft Plaque in CTA imaging

are segmented, we can follow two different approaches to detect/segment the soft plaque. These methods are applied in the region in the neighborhood of the vessel wall because the soft plaque always appears near the vessel walls. The schematic flow chart for the detection of the soft plaque is provided in the Figure 7.

Yang *et al.* used a harmonic skeletonization method [14] to calculate the axis of the segmented coronary arteries and the cross sectional areas along the axis. The cross sectional areas were then analyzed to estimate the location of stenosis along the axis of the vessel. This method does not give the location of the soft plaque along the walls of arteries. Moreover, there is no significant change in the cross sectional area during the initial stages of the plaque formation. Hence this method is not very effective for identifying the plaque deposits during the initial stages. These problems are overcome by the two methods proposed in Chapter 3 and Chapter 4.

In Chapter 3, we present a method for the automatic detection of the soft plaque by exploiting the structural properties (morphology) of the soft plaque. The soft plaque, as it grows larger starts occluding the blood flow in the coronary arteries and results in the reduction in the cross sectional area of that part of the coronary artery. Topologically, it results in the formation of local convexities in the artery walls, in

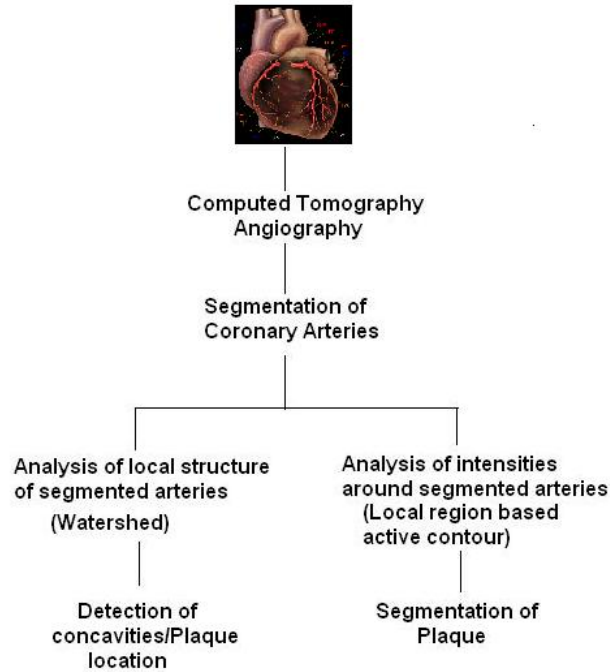


Figure 7: Detection of Soft Plaque

other words it results in local concavities in the blood lumen. We detect the resulting concavity to identify the location of the soft plaque.

In Chapter 4, we will discuss the importance of local region based active contours in finding significant local minima and segmenting images without making global assumptions. We briefly go through the mathematics behind these local region based active contours and show how this technique has been effectively used to segment the soft plaque from the CTA images. While using a region based energy in a local context, we have a number of choices for the energy. We used a most popular region based energy for the purpose of detection of soft plaque.

CHAPTER II

SEGMENTATION OF CORONARY VESSELS

For the purpose of segmentation of the coronary arteries, we make a reasonable assumption that the coronary vessels are cylindrical structures (at least locally around a small neighborhood). In other words, we have a 3D volume of CTA data that have a set of white voxels which are approximately arranged in an cylindrical shape. The problem now amounts to the detection of these voxels. The vessels can be aligned in any direction in the 3D space (i.e., their cylindrical axis may not necessarily be aligned along the major axes of the space, namely X, Y and Z). The vessels might also curve naturally as they descend along the walls of the heart. Hence it is necessary to treat the vessel as a piecewise cylindrical structure. The algorithm to detect the vessels must be independent of the direction of the cylindrical axes of the vessel and must take in to account the natural curvature of the vessel axis.

2.1 Vessel Filter

The vessel identification block can be described as a filter which takes the whole 3D volume as input and gives the set of voxels along the walls of the vessel as output. Now let us imagine a cylinder whose cylindrical axis is aligned along the Z-axis. Let the surface of the cylinder and the interior of the cylinder be white in color and everywhere outside the cylinder be black in color. Now let us find the difference (i.e., gradient) between the intensity of voxels in the 3D volume in X, Y and Z direction. The pattern of the gradient inside, along and outside the walls of the cylinder is given in Table 1.

Hence in the ideal example in the above case, the voxels along the walls of the vessel are the voxels that have non-zero difference along the X and Y directions. In

Table 1: Possible patterns of the gradient

Along X	Along Y	Along Z	Voxel location
0	0	0	Inside Cylinder
+/-ve	+/-ve	0	Along and neighboring the walls of cylinder
0	0	0	Outside Cylinder

the real scenario the problem is more complicated as mentioned in the introduction of this Chapter. Specifically:

1. The vessel is not globally cylindrical, but is piecewise cylindrical (meaning the vessel's central axis is curved along the walls of heart).
2. The axis of the piecewise cylinders are not necessarily aligned along the major axes (X, Y or Z).

Thus our filter should be able to detect the piecewise cylinders and should detect them irrespective of the alignment of their cylindrical axis. To do this we first calculate the second order derivatives of the intensity values to form a Hessian matrix for each voxel. The matrix is given as:

$$\nabla^2 I(\mathbf{x}) = \begin{bmatrix} I_{xx}(\mathbf{x}) & I_{xy}(\mathbf{x}) & I_{xz}(\mathbf{x}) \\ I_{yx}(\mathbf{x}) & I_{yy}(\mathbf{x}) & I_{yz}(\mathbf{x}) \\ I_{zx}(\mathbf{x}) & I_{zy}(\mathbf{x}) & I_{zz}(\mathbf{x}) \end{bmatrix}, \quad (1)$$

where $\mathbf{x} = (x, y, z)$ are the coordinates of any voxel in the 3D space and $I_{xx}(\mathbf{x})$, $I_{xy}(\mathbf{x})$, $I_{yy}(\mathbf{x})$ etc are second order partial derivatives of I . Note that the image has to be denoised by using a Gaussian or edge preserving smoothing filter [17] before calculating the Hessian matrix.

We then calculate the major modes of variations ie. the eigenvalues of the Hessian matrix in (1). These eigenvalues (λ_1 , λ_2 and λ_3) characterize the changes in the three

orthogonal directions irrespective of the choice of the X, Y, Z axis and thus helps in achieving directional independence while filtering for cylindrical shapes. More detail regarding the the relationship between different combinations of the eigenvalues and their corresponding possible 3D patterns was studied by Frangi *et al.* [15] and has been summarized in (Table 2). Recall that the coronary arteries appear as bright tubular structures in the CTA images. If the eigenvalues are such that λ_1 is approximately zero, and λ_2 and λ_3 are negative numbers with high absolute values then the corresponding voxel is supposed to be on the surface of the coronary artery. In other words:

$$\begin{cases} 0 \approx |\lambda_1| \ll |\lambda_2| \leq |\lambda_3|, \\ \lambda_2 < 0, \lambda_3 < 0. \end{cases} \quad (2)$$

Table 2: Possible patterns in 3D, based on eigenvalues from Hessian matrix. Adapted from [15].

λ_1	λ_2	λ_3	orientation pattern
N	N	N	noisy, no preferred direction
L	L	H-	plate-like structure (bright)
L	L	H+	plate-like structure (dark)
L	H-	H-	tubular structure (bright)
L	H+	H+	tubular structure (dark)
H-	H-	H-	blob-like structure (bright)
H+	H+	H+	blob-like structure (dark)

Here “H” means High absolute value and “L” means Low absolute value. + denote positive value and - denotes negative value.

The mathematical formulation of the filter that gives a larger response to the pattern of Eigenvalues that denote the corresponding cylindrical shape was given by Frangi *et al.* [15] as follows:

$$M(\lambda_1, \lambda_2, \lambda_3) = \begin{cases} 0, & \text{if } \lambda_2 > 0 \text{ or } \lambda_3 > 0 \\ (1 - \exp(-\frac{R_A^2}{2\alpha^2}))(\exp(-\frac{R_B^2}{2\beta^2}))(\exp(-\frac{T^2}{2\gamma^2})), & \text{Otherwise} \end{cases} \quad (3)$$

Where,

$$R_A = \frac{|\lambda_2|}{|\lambda_3|}$$

$$R_B = \frac{|\lambda_1|}{\sqrt{|\lambda_2\lambda_3|}}$$

$$T = \sqrt{\lambda_1^2 + \lambda_2^2 + \lambda_3^2}$$

and $\alpha = \beta = 0.5$ and $\gamma = 10$

The response of this Hessian based filter for any voxel takes in to account the image characteristics in a small neighborhood around that voxel and is naturally suitable for identifying cylinder-like structures. The result of the Hessian filter on 2 datasets have been shown in Figure 8.

2.2 Active Contour based segmentation

Active contours are very popular and efficient techniques for the segmentation of required data from the images. The physical motivation behind these techniques is to allow a closed curve or surface to deform continuously under the influence of the internal and external forces. While smoothness is enforced by the internal forces, the external forces from the image data push the contour towards the desired image features that need to be segmented. Two popular active contour models are based on the type of energy that is defined using the image data. These models are as follows:

2.2.1 Edge based active contours

In the edge based active contour models, the contour evolves on an energy that has a minimum along the edges of the object that needs to be segmented. The equation for the energy is given as follows:



Figure 8: Results of the Hessian Filter

$$E = \oint_{C(s)} g(I) ds \quad (4)$$

Where, g is a positive, strictly decreasing function calculated from the image data, C is the active contour and s is the arc length parameter. One nice example of the function g can be calculated from J , a Gaussian smoothed version of the image I as

follows:

$$g = \frac{1}{1 + \|\nabla J\|^2} \quad (5)$$

We obtain the following curve shortening flow, by taking the first variation of the Energy functional given in the Equation 4 [16] [19].

$$\frac{\partial C}{\partial t} = g\kappa\mathcal{N} - \nabla g \quad (6)$$

where κ is the curvature of the curve and \mathcal{N} is the inward unit normal to the curve.

We can add a inflation term, ν to the above equation. When ν is negative the curve tends to grow in the outward direction by countering the effects of the curvature term. The updated partial differential equation is as given below:

$$\frac{\partial C}{\partial t} = g(\kappa + \nu)\mathcal{N} - \nabla g \quad (7)$$

When the initial contour is updated based on the above partial differential equation which is based on an edge based energy as given in the Equation 4, the contour locks itself at strong edges where the internal curvature based energy balances the image gradient based external energy and thus results in the segmentation of the desired object.

2.2.2 Region based active contours

This model does not rely on the gradient of the image data for stopping the evolving curve. Instead it minimizes the energy based on the image intensities inside and outside the evolving curve for stopping the evolution. A famous example of region based active contour is the Chan-Vese model [26] which is based on the Mumford-Shah model [25]. The energy function proposed by Chan and Vese is as follows:

$$E = \int_{\Omega} (I - u)^2 dA + \int_{\bar{\Omega}} (I - v)^2 dA \quad (8)$$

Here, I is the image data, u and v represent the mean intensity values over the regions Ω and $\bar{\Omega}$ respectively. Ω and $\bar{\Omega}$ are the region interior and exterior of the evolving curve. The minimum energy is obtained when the mean image intensities in the region inside and outside the evolving contour is closely approximated by u and v .

The curve shortening solution based on the above region based energy will become apparent after the discussion of the level set techniques in the next section.

2.3 Level set technique

2.3.1 Explicit and implicit representations of curves

Mathematically a curve can be represented explicitly or implicitly. The explicit representation is based on a parametrization of the following type:

$$C(p) : [0, 1] \rightarrow \mathbb{R}^2, \quad (9)$$

where p can be any parameter. This is equivalent to:

$$C(p) \doteq [x(p), y(p)]^T = X(p). \quad (10)$$

$C(p)$ is said to be a *closed curve* if $C(0) = C(1)$ and $C'(0) = C'(1)$

Different schemes for the evolution of parametric curves was proposed by Kass *et al.* [27] and Yuille *et al.* [28], where the parametric curves are represented using splines. The parametric representation of curves provide a lot of numerical implementation challenges which are over come by using the implicit representation of the curves.

In the implicit notation, the curve is represented as the zero set of two-dimensional function. This leads to the powerful level set technique of Osher and Sethian [10] [11] [12]. The idea is to look at all the level curves of the aforementioned 2D function.

Explicitly, let $f : \mathbb{R}^2 \rightarrow \mathbb{R}$ be a smooth Lipschitz continuous function. We then represent the curves by

$$\{(x, y) \in \mathbb{R}^2 : f(x, y) = k\}, \quad (11)$$

and the original curve is the zero level set where $k = 0$.

An example of level set function is a *signed distance function* whose value is zero along the contour of the curve, negative inside the curve and positive outside the curve. The level set representation of a curve C is given by the following equation:

$$\psi(x) = \begin{cases} -\inf_{y \in C} d(x, y), & \text{if } x \in \Omega \\ 0, & \text{if } x \in C \\ +\inf_{y \in C} d(x, y), & \text{if } x \in \mathbb{R} \setminus \Omega \end{cases} \quad (12)$$

where Ω is the interior of the closed curve C and $d(x, y)$ is the Euclidean distance function.

The level set representation of curves (refer Figure 9) has many advantages including the simplification of the numerical implementation by avoiding complex re-sampling schemes of control points, natural handling of topological changes (splitting and merging) of the evolving curve and easy generalization to higher dimensional objects like the surfaces in \mathbb{R}^3 . Moreover, the geometric properties of the curve can be easily estimated using the level set representation.

2.3.2 Level set representation of active contour models

As mentioned in the previous section, it is easier to calculate the geometric properties (say, κ) of a curve in a discrete domain by using the level set representation of the curve. Hence, the level set representation of the geometric curve evolution equation (Equation 7) is given as follows [10] [11]:

$$\frac{\partial \Psi}{\partial t} = g(\operatorname{div} \left(\frac{\nabla \Psi}{\|\nabla \Psi\|} \right) + \nu) \|\nabla \Psi\| + \nabla g \cdot \nabla \Psi. \quad (13)$$

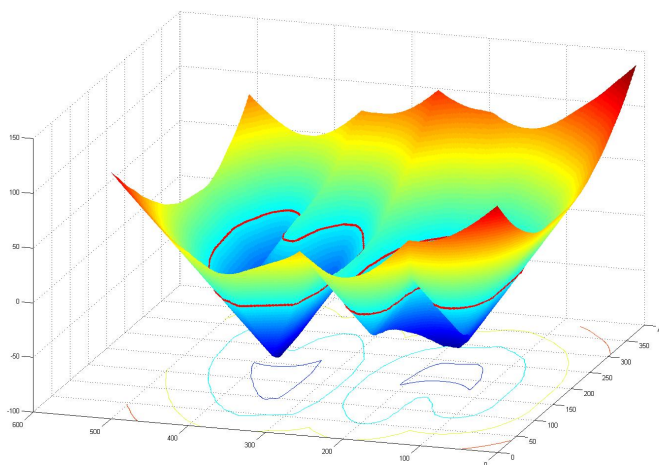
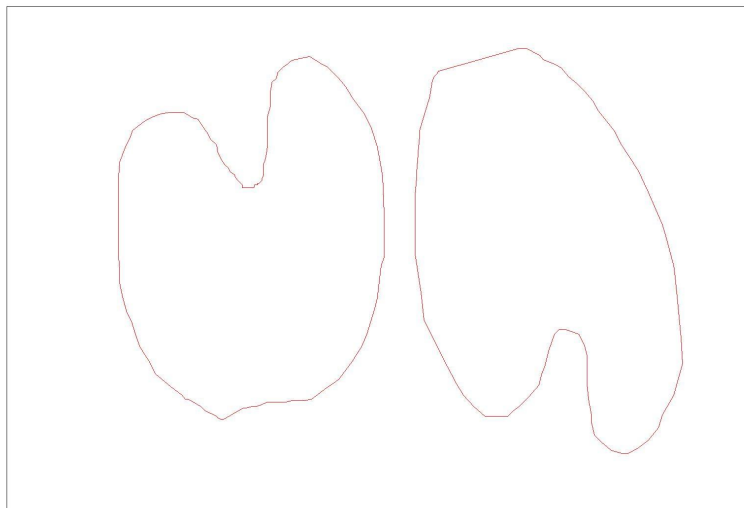


Figure 9: A closed curve(Left) and its Level set representation(Right)

Now let us see the level set version of region based active contours. Let ψ be the level set representation of the active contour. We define the Heaviside function H and Dirac function δ_0 as follows:

$$H(z) = \begin{cases} 1, & \text{if } z \geq 0 \\ 0, & \text{if } z < 0 \end{cases}, \quad \delta_0(z) = \frac{d}{dz}H(z) \quad (14)$$

The region based curve evolution equation based on the energy defined by the

equation 8 is given as:

$$\frac{\partial \Psi}{\partial t} = \delta_\epsilon(\Psi)[-(I - u)^2 + (I - v)^2], \quad (15)$$

where δ_ϵ is a numerical approximation of Dirac function, u and v are the average intensities inside the contour and outside the contour respectively. The formula for calculating u and v are given as (more details regarding the derivation can be found in [26]):

$$u(I, \Psi) = \frac{\int_{\mathbb{R}^2} H(\Psi) I dA}{\int_{\mathbb{R}^2} H(\Psi) dA} \quad (16)$$

$$v(I, \Psi) = \frac{\int_{\mathbb{R}^2} (1 - H(\Psi)) I dA}{\int_{\mathbb{R}^2} (1 - H(\Psi)) dA} \quad (17)$$

2.4 Bayesian based active surface segmentation

For the purpose of segmentation of the coronary arteries from the CTA data we use the concepts of edge based active contours. But instead of using an energy based on the image gradient, we employed an energy based on the Bayesian posterior probabilities of the voxels. The filter response of the Hessian based vessel filter (see Section 2.1) is noisy and not smooth. In order to achieve a smooth vessel segmentation, we utilized the Bayesian driven level set based active contour model proposed by Yang *et al.* [13]. The initialization for the segmentation is obtained by computing a “vesselness” measure of the eigenvalues of the Hessian matrix from the image, as discussed in section 2.1. The initial level set (signed distance function as in Equation 21) from the shape prior is evolved based on the following equation [16] [19]:

$$\frac{\partial \Psi}{\partial t} = \phi \left(\operatorname{div} \left(\frac{\nabla \Psi}{\|\nabla \Psi\|} \right) + \nu \right) \|\nabla \Psi\| + \nabla \phi \cdot \nabla \Psi. \quad (18)$$

Here ν is the inflationary term for evolving the level set in the outward direction. ϕ is the conformal factor calculated based on the posterior probabilities of the image

voxels as follows [13]:

$$\phi(\mathbf{x}) = (Pr^*(\mathbf{x} \in c_{in}) - Pr^*(\mathbf{x} \in c_{out}))^2, \quad (19)$$

where class c_{in} represents the object to be segmented, and class c_{out} represents the background.

If the image data has more than two classes, then we take the conformal factor as the squared difference of the largest two posterior probability of the voxel. The posterior probability is calculated based on the following equation:

$$Pr(\mathbf{x} \in c_k | I(\mathbf{x}) = v) = \frac{Pr(I(\mathbf{x}) = v | \mathbf{x} \in c_k) Pr(\mathbf{x} \in c_k)}{\sum_{\gamma=1}^n Pr(I(\mathbf{x}) = v | \mathbf{x} \in c_\gamma) Pr(\mathbf{x} \in c_\gamma)}, \quad (20)$$

where I is the image and c_k is one of the n classes. The prior probabilities are estimated using EM algorithm [32] [33].

The result of the level set evolution according to Equation 18 segments the lumen of the coronary arteries from the CTA images. The level set evolution over the conformal factor computed using the Bayesian posterior probabilities is able to segment out the blood lumen, while still preserving the concavities created due to the soft plaque deposits. The result of the Bayesian active contour model based segmentation for 2 datasets are shown in Figure 10.

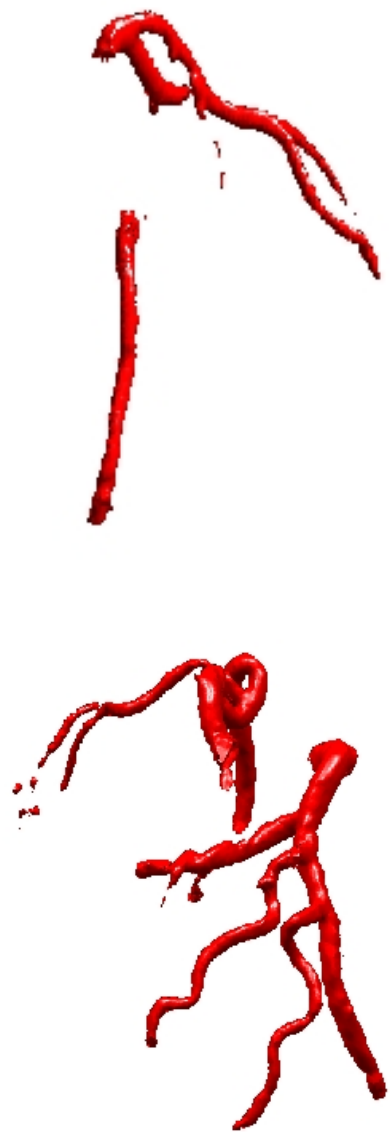


Figure 10: Results of Bayesian active contour segmentation

CHAPTER III

WATERSHED BASED DETECTION OF SOFT PLAQUE

As mentioned earlier, the soft plaque invades the area of the blood lumen resulting in the formation of concavities in the blood lumen. The segmentation result from chapter 2 provides the walls of the blood lumen. If we are able to detect these local concavities in the segmented blood lumen, it means that we can detect the presence of soft plaque. This chapter describes a method that is used to detect the approximate location of the concavities (*i.e.* soft plaque) along the walls of the blood lumen and the results of this method.

3.1 Local convexity Vs Global convexity

Let \mathbf{A} be a connected set in \mathbb{R}^n . Intuitively, if a line segment through any two points in the set \mathbf{A} lies in \mathbf{A} itself, then \mathbf{A} is said to be convex [9]. In other words, \mathbf{A} is said to be convex if $\forall \lambda, \mu \geq 0$ and $\lambda + \mu = 1$:

$$\lambda x + \mu y \in \mathbf{A}, \forall x, y \in \mathbf{A}.$$

Let \mathbf{A} be the set of all voxels classified as the blood lumen. Then \mathbf{A} contains all the voxels on the surface of the lumen segmented using the level set Equation 18, and all the points that lie in the interior of the surface. In other words, \mathbf{A} is the set of all voxels with 0 or negative value in the final level set that was evolved based on Equation [18]. In \mathbb{R}^3 , the set \mathbf{A} is a tubular, tree like structure and \mathbf{A} is definitely not convex, because the center line(axis or skeleton) of the tubular structure has a curvature. Hence $\exists \lambda, \mu \geq 0$ and $\lambda + \mu = 1$ such that:

$$\exists x, y \in \mathbf{A} \text{ and } \lambda x + \mu y \notin \mathbf{A}.$$

The individual branches of the coronary artery tree need not be convex. Hence it is not possible to directly apply this property of convex sets to detect the concavities in the blood lumen. The immediate idea that comes to mind is to decompose the center lines into piece-wise linear components. The axis of piecewise linear tubular structures have zero curvature, and hence it is possible to detect the concavities using the above properties of the concave sets. However this method will not work well, if the radius of curvature of the local concavities is comparable to that of length of the piece-wise cylinder. Hence there is a need for a technique to detect the local concavities in a set that is not globally convex, but is (in crude terms) piecewise convex. In the subsection 3.3, we will talk about the general idea of our technique applied to 2D synthetic dataset for the detection of the concavities and we will discuss the result of this technique when applied for identifying the concavities in the blood lumen.

3.2 Watershed transformation

A *watershed* refers to a region (a ridge or crest line) that divides two drainage areas (river or stream or lake). A drainage area is often referred to as the catchment basin [18]. The watershed transform identifies the catchment areas in a domain by taking the depth information as the input. It can be used for segmentation of the images if we are able to represent the content of interest and background in the image in to catchment basins and watersheds.

Consider an image as shown in Figure 11. Let us imagine an application for which we have to segment the dark regions. In order to use the watershed transform for our segmentation, we need to define an energy where the brighter intensities denote higher energy and the darker intensities denote lower energy (in other words, white indicates maximum possible energy (say 1) and black indicates zero energy). Then the energy representation in the form of a surface in 3D looks as shown in the Figure 12 (image is

taken from Mathworks.com). The catchment and the watershed lines for this energy are shown in the figure. The region of interest can be segmented by identifying the catchment regions in the defined energy using watershed transform [21, 22].

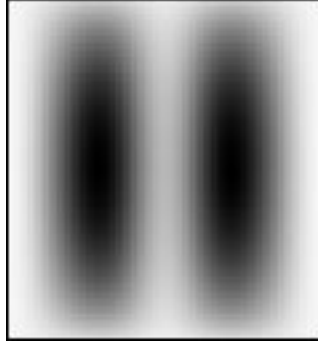


Figure 11: A 2D energy representation of catchment basins

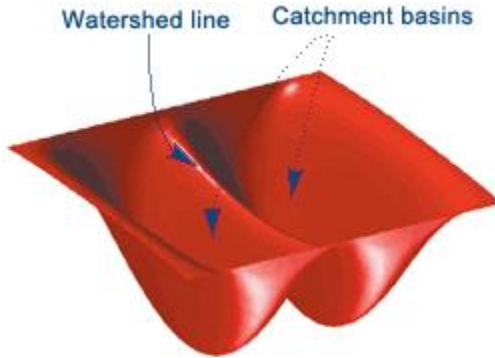


Figure 12: A 3D surface representation of the energy shown in figure 11

3.3 Automatic detection of local concavity

Let \mathbf{A} be a simply connected set of points in \mathbb{R}^3 . It is possible to represent the \mathbf{A} as a level set which is zero along the boundary of \mathbf{A} (denoted by $\partial\mathbf{A}$), negative in the interior of \mathbf{A} and positive elsewhere. One good function that transforms \mathbf{A} in to such a level set is the signed distance function as given in the following equation:

$$\Psi^0(x) = \begin{cases} - \inf_{y \in \partial\mathbf{A}} d(x, y) & \text{if } x \in \mathbf{A} \\ + \inf_{y \in \partial\mathbf{A}} d(x, y) & \text{if } x \notin \mathbf{A} \end{cases} \quad (21)$$

where $d(x, y)$ denotes the usual Euclidean distance.

Let $C^0(p)$ be the closed surface that represents $\partial\mathbf{A}$, the boundary of \mathbf{A} . Let \mathbf{A} have local concavities, which result in local changes in the radius of curvature on C . To detect these concavities it is better to work in the set that is complement of \mathbf{A} in \mathbb{R}^3 . But this complement is unbounded and hence is not a good set to work with. Hence it becomes necessary to derive a bounded set out of the complement. Let t be the imaginary time variable. Consider a closed curve $C^t(p)$, such that, the region between $C^0(p)$ and $C^t(p)$ is bounded and belongs to the complement of \mathbf{A} . One solution for $C^t(p)$ is the curve evolved according to the following equation:

$$\frac{\partial C^t(p)}{\partial t} = -\mathcal{N}, \quad (22)$$

where \mathcal{N} is the inward normal to the curve $C^t(p)$. The level set version of the Equation 22 is as follows [10] [11]:

$$\frac{\partial \Psi^t}{\partial t} = -\|\nabla \Psi\|. \quad (23)$$

Note that evolving the initial level set from Equation 21 according to the Equation 23 is equivalent to performing dilation on the contour $C^0(p)$. The Equation 22 evolves the curve, $C^0(p)$ in the direction of the outward normal to the curve. This evolution, in addition to dilating the curve, also smoothes any sharp curvature changes or concavities present in the curve. Hence after evolving for certain time t , the resultant curve $C^t(p)$ is a dilated and curvature smoothed version of the initial curve. This is followed by eroding the curve so that the final contour is still a dilated and curvature smoothed version of the initial curve, but has its length comparable to that of the initial curve. For the purpose of erosion we can use the following level set equation:

$$\frac{\partial \Psi^t}{\partial t} = \|\nabla \Psi\|. \quad (24)$$

The above equation has very little effect on the curvature which was smoothed by the dilation operation performed by the Equation 23.

Now let us define a set \mathbf{B} as follows:

$$\mathbf{B} = \{x \in \mathbb{R}^3 : \Psi^t(x) \leq 0\} \cap \text{Complement}(\mathbf{A}), \quad (25)$$

where \mathbf{B} is the (bounded) set of all points in between the zero level of the initial level set and that of the final level set which is the result of the evolution based on Equation 23 and Equation 24. Now $C^0(p)$ and $C^t(p)$ are closed curves and are the 2 boundaries of the set \mathbf{B} and we are interested in finding the concavities along the boundary represented by the curve $C^0(p)$.

Next Let \mathbf{D} be the distance of the points in set \mathbf{B} from the boundary of \mathbf{B} (denoted by $\partial\mathbf{B}$):

$$\mathbf{D}(x) = \begin{cases} - \inf_{y \in \partial\mathbf{B}} d(x, y) & \text{if } x \in \mathbf{B} \\ 0 & \text{elsewhere} \end{cases} \quad (26)$$

where $d(x, y)$ is the usual Euclidean distance.

It can be seen that the maximum value of \mathbf{D} for any $x \in \mathbb{R}^3$ is 0. Intuitively, the minimum value of \mathbf{D} occurs at the vicinity of the concavity in the boundary of \mathbf{B} represented by $C^0(p)$ (this is because, the length of $C^0(p)$ and $C^t(p)$ are comparable). This minimum serves as the catchment basins for the watershed transform [21] when applied to the function \mathbf{D} . When watershed transform is applied in the discrete domain (as in [22]), it results in identifying a number of catchment region. A suitable threshold (for the area/volume of the catchment region) can be applied to identify the largest catchment regions that directly correspond to the concavities in the boundary represented by $C^0(p)$.

3.4 Results and Discussion

The results for two dimensional examples using the scheme discussed in the previous subsection are shown in Figures 13–16. In the first example, there is a concavity

present in the circular object. The second example is that of a synthetic 2D vessel with a stenosis. For both the examples, the watershed scheme was able to identify the concavities. For the purpose of detection of soft plaque in 3D CTA volumes, we had a set of 8 datasets for which the expert radiologists had marked the approximate location of the soft plaque. Out of these 8 datasets, 2 datasets had soft plaque deposits that resulted in significant reduction of the cross sectional area of the arteries. We applied the watershed scheme in 3D and were able to locate the approximate location of the soft plaque along the walls of the coronary artery. The results for the 2 datasets can be seen in Figure 17 and Figure 18. In the results, the blue surface indicates the walls of the blood lumen and the red surface indicates the approximate location of the plaque.

The time for the computation of morphological operations, distance function and watershed transform in 3D is high. The narrow band [20] and fast marching[35] approaches were used to reduce the computation time. The main problem of the convexity based approach for the detection of the soft plaque is that it does not perform well in identifying plaque deposits that are small in volume, which is usually the case during the initial stages of the plaque. Another issue is that it does not provide the actual segmentation of the plaque, instead it just gives the approximate location of the plaque. These problems are overcome by the hybrid active contour scheme proposed in the Chapter 4.

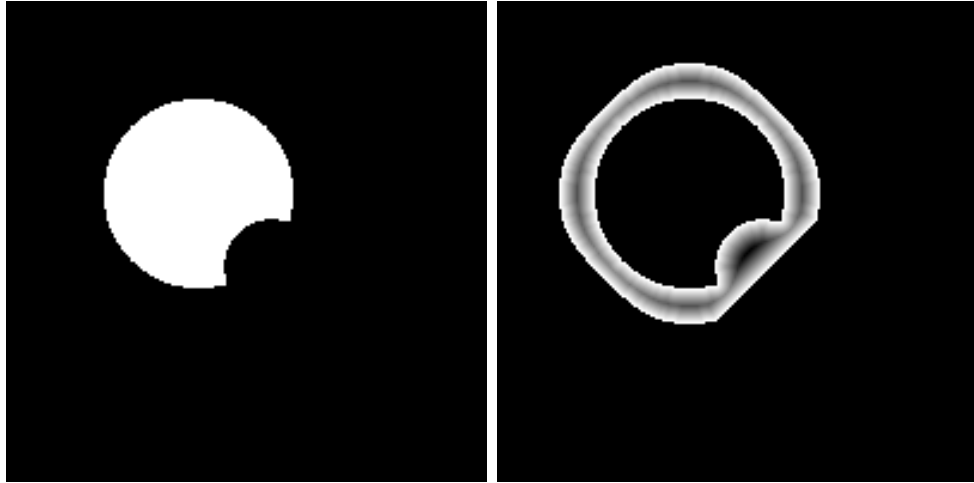


Figure 13: A 2D object with concavity (Left). The distance function calculated in the region between the object boundary and the dilated and 'curvature-smoothed' object boundary (Right).

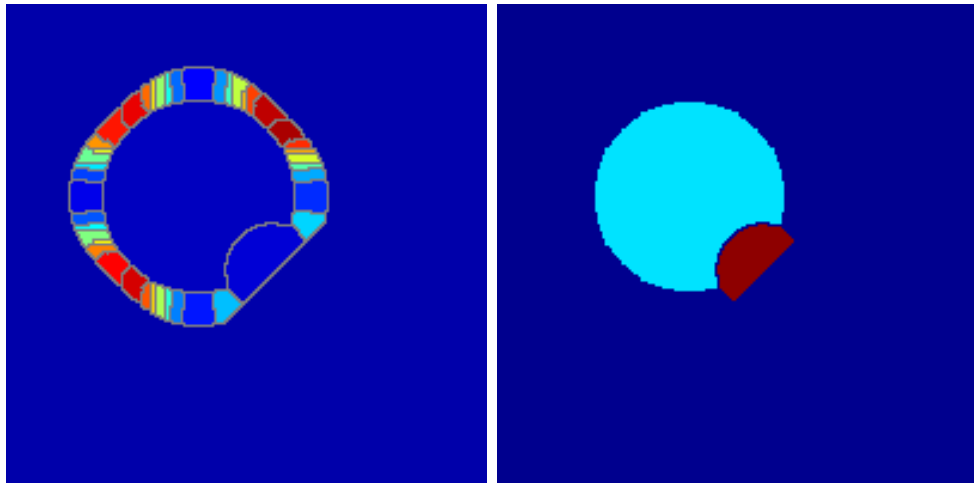


Figure 14: Results of identification of concavity (for object in Figure 13). This image shows the watershed catchment areas (Left) and the largest catchment area indicates the concavity in the boundary (Right).

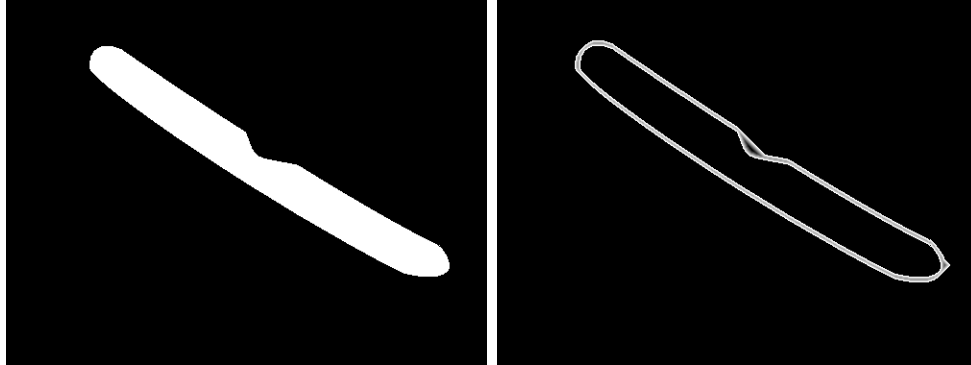


Figure 15: A 2D synthetic vessel with concavity (Left). The distance function calculated in the region between the object boundary and the dilated and 'curvature-smoothed' object boundary (Right).

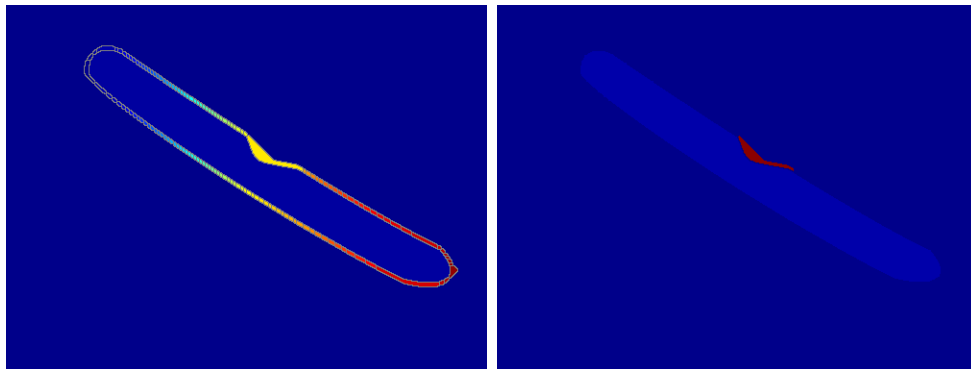


Figure 16: Results of identification of concavity (for object in Figure 15). This image shows the watershed catchment areas (Left). The largest catchment area indicates the concavity in the boundary (Right).

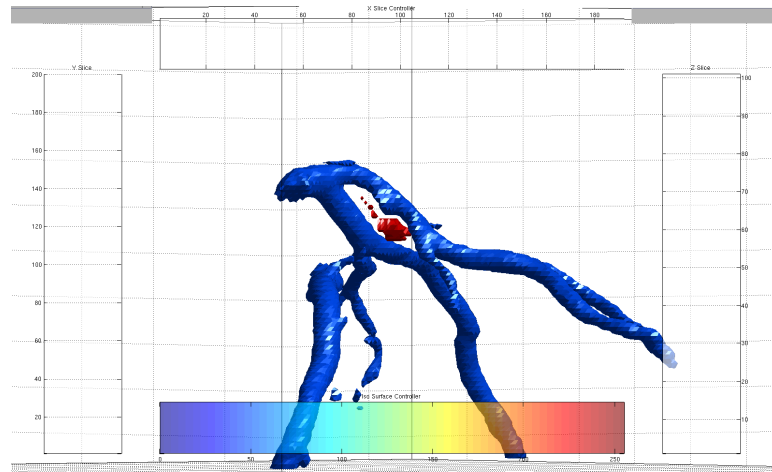


Figure 17: Results of identification of soft plaque deposits in coronary arteries of dataset 1. The Red color surface indicates the approximate location of the plaque.

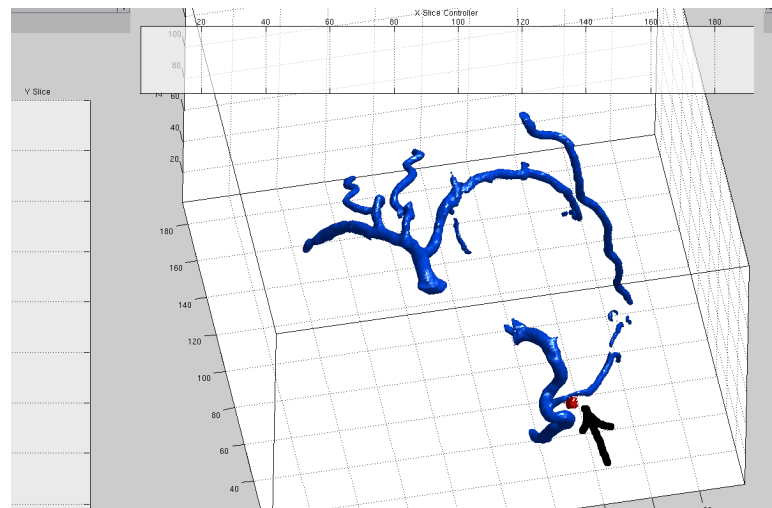


Figure 18: Results of identification of soft plaque deposits in coronary arteries of dataset 2. The Red color surface indicates the approximate location of the plaque.

CHAPTER IV

LOCAL REGION BASED SEGMENTATION

In this section, we will describe a technique used to segment the soft plaque by using the intensity properties of the soft plaque. In the datasets for which the ground truth (location of soft plaque) is known, we noted that the the plaque has an intensity distinct from that of the blood and the cardiac muscle. However the volume of the plaque is small and a traditional active contour methods are not robust enough to segment the plaque volume separately.

4.1 Segmentation issues with traditional energy schemes

As mentioned in Section 2.2, the traditional active contour segmentation methods are broadly categorized into edge based and Region based schemes. In this section, we will discuss the drawbacks of these energy schemes that make it tough to use them for the purpose of detection of soft plaque from CTA images.

4.1.1 Edge based energy

When the boundary of the object is marked by a strong image gradient, the problem of finding the boundary is equivalent to finding the local minimum cost closed curve on a conformal Euclidean metric [16] [19]. As discussed in Section 2.2.1, the initial curve is evolved based on the equation obtained by the gradient descent method applied on the following energy equation:

$$E = \oint_{C(s)} g(I) ds, \quad (27)$$

where g is a positive, strictly decreasing function calculated from the gradient of the Gaussian smoothed version (J) of the image I as follows:

$$g = \frac{1}{1 + \|\nabla J\|^2}. \quad (28)$$

In CTA images, along the walls of the coronary arteries, the contrasts between soft plaque & blood lumen and soft plaque & cardiac muscle are very low and hence the gradient calculated at the edges of soft plaque and the blood lumen/cardiac muscle is very weak. Hence, the edge based geodesic active contour method does not provide good segmentation results for the segmentation of the soft plaque.

Another popular edge based energy is the energy calculated from Bayesian posterior probabilities of the pixel intensities as discussed in Section 2.4. The intensity of the soft plaque lie exactly at the region overlapping the intensity of the blood lumen and the cardiac muscle (as shown in Figure 19) and it is not possible to separate the histogram from CTA images to differentiate between the blood, plaque and muscle intensities. Hence, the posterior probabilities cannot be used in the edge based scheme to segment the soft plaque.

4.1.2 Region based energy

The region based active contours models can detect objects whose boundaries are not necessarily defined by gradient. The stopping term of the evolving contour in these models is based on particular properties that can partition the image into two or more distinct regions. A famous example of region based active contour is the Chan-Vese model [26] which is based on the Mumford-Shah model [25]. As mentioned in Section 2.2.2, the energy function proposed by Chan and Vese is as follows:

$$E = \int_{\Omega} (I - u)^2 dA + \int_{\bar{\Omega}} (I - v)^2 dA. \quad (29)$$

Here, I is the image data, u and v represent the mean intensity values over the regions Ω and $\bar{\Omega}$ respectively. Ω and $\bar{\Omega}$ are the region interior and exterior of the evolving

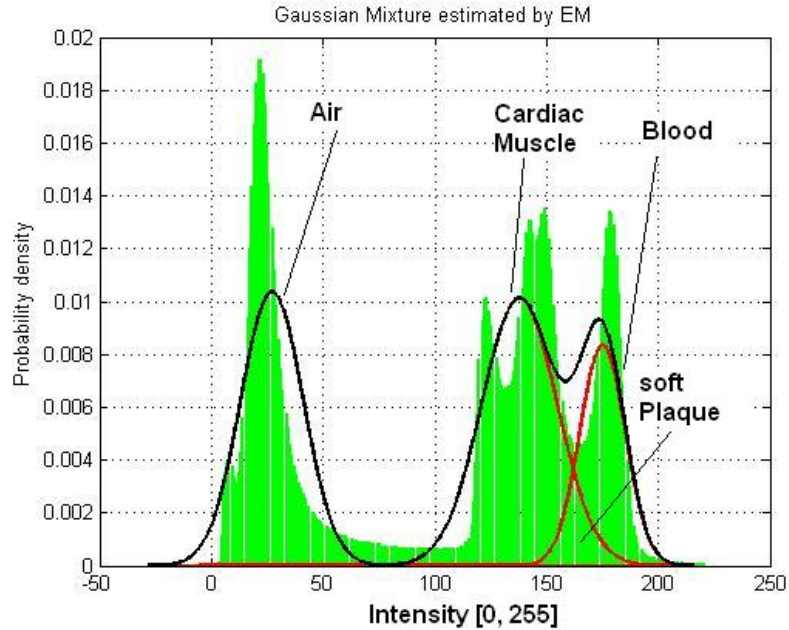


Figure 19: Soft plaque intensity in the region of overlap identified by EM algorithm [32] [33].

curve. The minimum energy is obtained when the mean image intensities in the region inside and outside the evolving contour is closely approximated by u and v .

It can be seen that the definition of the energy takes in to account the intensity properties of the whole domain. The mean intensities of the blood lumen and the cardiac muscle are easily separable. However as mentioned in the previous section, the intensity ranges of soft plaque lies in the region of overlap of the blood and muscle intensities and the mean intensity of plaque lies between the mean intensities of the blood and the muscle. Moreover, the plaque deposits are smaller in volume compared to that of the blood lumen. Hence while it is possible for the above region based model to segment the blood lumen from the muscle, it is challenging to segment the plaque deposits from the lumen and the muscle.

In the next section, we will discuss a hybrid energy scheme that we used to segment the soft plaque from CTA images.

4.2 Local Region based energy

The above shortcomings of the tradition energies are overcome by using an energy scheme proposed by Lankton *et al* [23]. This energy scheme is a hybrid energy scheme and uses the principles of geodesic active contours and region based active contours. It is similar to a geodesic active contour because it is essentially a curvature flow. However the energy used for the curve shortening depends on the intensity of pixels in a small neighborhood around the evolving contour. The energy function for these hybrid active contour scheme is defined as follows:

$$E = \oint_{C(s)} \check{g}(I, s) ds, \quad (30)$$

where $\check{g}(I, s)$ is a function that depends on the image properties corresponding to the small neighborhood around the evolving contour given by $C(s)$. We can notice that the Equation 30 is very similar to the geodesic active contours given by Equation 27 (which is same as Equation 4). The difference is in the nature of the function used for calculating the energy for the minimization problem.

4.2.1 Examples of Local Region based Energy

For the purpose of hybrid scheme, the function $\check{g}(I, s)$ can be based on the Bhattacharya measure [29, 30, 31] as given in Equation (31) or it can be based on Chan and Vese model as given in Equation (32), or other region based models like the one proposed by Yezzi *et al* [24] as given in Equation (33).

We will use the following notation in the sequel:

The region $\omega(s)$ be defined as $\Omega \cap B_r(C(s))$ which is the intersection of the Ω , interior of the curve C with the small neighborhood $B_r(C(s))$ which is nothing but a Ball of radius r with center as $C(s)$. Similarly, let $\bar{\omega}(s)$ be $\bar{\Omega} \cap B_r(C(s))$ which is the intersection of the exterior of the curve with the small neighborhood around $C(s)$ (as shown in Figure 20).

$A_{in}^l(s)$ and $A_{out}^l(s)$ denote the areas of small neighborhoods inside the contour and outside the contour, respectively. They are given by the following equations:

$$A_{in}^l(s) = \int_{x \in \omega(s)} dx,$$

$$A_{out}^l(s) = \int_{x \in \bar{\omega}(s)} dx.$$

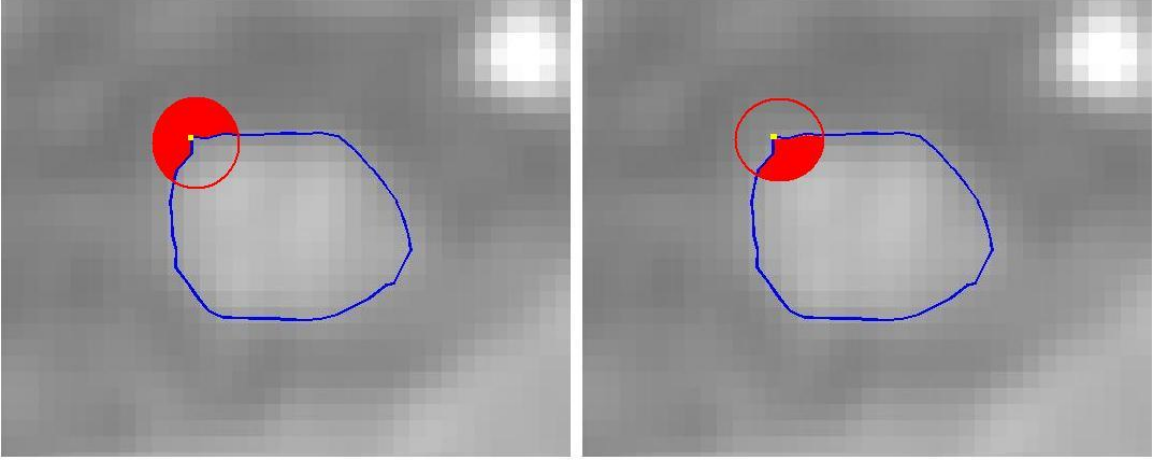


Figure 20: The exterior and interior of local neighborhood regions. The Yellow dot corresponds to $C(s)$. Red Ball corresponds to $B_r(C(s))$

The local energy function based on Bhattacharya coefficient is given as follows:

$$\check{g}(I, s) = \int_{z \in \mathbb{Z}} \sqrt{P_{in}(z, s) P_{out}(z, s)} dz, \quad (31)$$

where

z is the intensity variable.

$P_{in}(z, s)$ and $P_{out}(z, s)$ are the probabilities of the intensity z to be found in the small neighborhood region, inside and outside the curve C . They are given as follows:

$$P_{in}(z, s) = \frac{\int_{x \in \omega(s)} \delta(z - I(x)) dx}{A_{in}^l(s)},$$

$$P_{out}(z, s) = \frac{\int_{x \in \bar{\omega}(s)} \delta(z - I(x)) dx}{A_{out}^l(s)},$$

where δ is the Dirac delta function.

The local energy function based on Chan and Vese model is given as follows:

$$\check{g}(I, s) = \int_{x \in \omega(s)} (I(x) - u_l(s))^2 dx + \int_{x \in \bar{\omega}(s)} (I(x) - v_l(s))^2 dx \quad (32)$$

where

$u_l(s)$ and $v_l(s)$ are the mean intensities in the small neighborhood region, inside and outside the curve C and are given as follows:

$$\begin{aligned} u_l(s) &= \frac{\int_{x \in \omega(s)} I(x) dx}{A_{in}^l(s)}, \\ v_l(s) &= \frac{\int_{x \in \bar{\omega}(s)} I(x) dx}{A_{out}^l(s)}. \end{aligned}$$

The local energy function based on the model proposed by Yezzi *et al* [24] is as follows:

$$\check{g}(I, s) = -\frac{(u_l(s) - v_l(s))^2}{2}, \quad (33)$$

where $u_l(s)$ and $v_l(s)$ are the mean intensities in small neighborhood regions, inside and outside the curve C , respectively.

4.2.2 Curve shortening flow for Hybrid Energy

Now we can look at the solution of curve shortening flow for the energy defined in the Equation (30). Lankton *et al* derived the gradient descent equation for the hybrid scheme with the local region based energy being the Chan and Vese energy. As seen before, the energy in hybrid scheme looks like that of the geodesic active contour scheme. But the function inside the integral is dependent on the curve parameterization s . The flow is given as follows:

$$\frac{\partial C}{\partial t} = \check{g}(I, s) \kappa \mathcal{N} + T_1(I, s), \quad (34)$$

where $T_1(I, s)$ is the term due to the minimization of local region based energy that varies based on the parameter s . The derivations for the minimizations of specific

region based energies are given in [26, 29, 24] and can be easily plugged in to the term T_1 .

For the specific case where the local energy is based on Chan and Vese model, the curve evolution equation is given as follows [23]:

$$\begin{aligned} \frac{\partial C(s)}{\partial t} = & \left\{ \int_{x \in \omega(s)} (I(x) - u_l(s))^2 dx + \int_{x \in \bar{\omega}(s)} (I(x) - v_l(s))^2 dx \right\} \kappa \mathcal{N} - \\ & \left\{ \oint_{C(r) \cap B_r(C(s))} (u_l(r) - v_l(r))(2I - u_l(r) - v_l(r)) dr \right\} \mathcal{N}. \end{aligned} \quad (35)$$

The above gradient descent flow evolves every point along the curve based on the properties of the local region inside and outside the curve.

4.3 *Blob and Lung Correction*

In the heart, the coronary vessels occur in the proximity of the heart chamber and the epicardium (thus in proximity of lungs). The heart chambers are filled with blood and have a high intensity in the CTA data. The lungs are filled with air and have very low intensity in the CTA data. Hence while applying the local region based scheme to segment the soft plaque along the walls of the coronary artery, care must be taken to ensure that the blobs and the lungs are not included in the calculation of the energy function. This can be done by reducing the radius r involved in choosing the local neighborhood. Another effective and straight forward method is to identify the blob and the lung and fill it with the intensity of the cardiac muscle.

The first step is the identification of blob structures and the lung. For the process of identification, the following steps were used:

1. Used simple thresholding (where the threshold can be learned automatically from the histogram using Expectation Maximization [32] [33]) to threshold the blobs and lungs separately.
2. Morphological closing [34] was performed to eliminate the vessels present in the lungs.

3. Dilate the blob and the lung structures by using a circular structural element with a radius of 2 pixels. The resulting binary image differentiates between the cardiac muscle/coronary arteries and the blobs/lungs.

The next step is the filling of blob/lungs with the intensity values comparable to that of the cardiac muscle. This was achieved by using a fast marching scheme [35, 36]. Let us tag pixels that correspond to cardiac muscle/coronary arteries as *Alive* and other pixels that belong to blobs and lung as *Far*. The fast marching scheme for filling up the blobs and lungs is as follows:

1. Begin Loop1: If the number of *Far* pixels is not 0, then mark the *Far* pixels that are one grid point away from *Alive* pixels as *Close*, Else, STOP.
2. Begin Loop2: If the number of *Close* pixels is not 0, then pick any point in *Close* and call it *Trial*, Else, go to End Loop2.
3. Find average intensity value of all neighbor pixels of *Trial* that are *Alive*.
4. Assign the average value as the intensity of *Trial* and change its status to *Done*
5. Go to Begin Loop2.
6. End Loop2: Mark all the *Done* pixels as *Alive* and Go to Begin Loop1

This method of filling with the average intensity of its neighborhood pixels (which are that of cardiac muscle) ensures that the blobs and the lungs are filled in a smooth fashion without any sharp edges. The results of the above method for two datasets are given in Figure 21 and 22, respectively.

4.4 Segmentation Results

This section discusses the application of the hybrid active contour scheme discussed in 4.2 for the segmentation of soft plaque. As discussed in Chapter 2, the Bayesian

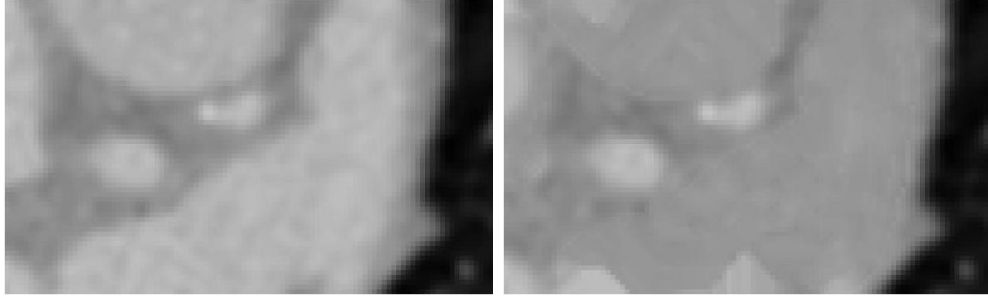


Figure 21: Dataset1: Before and After Blob Correction

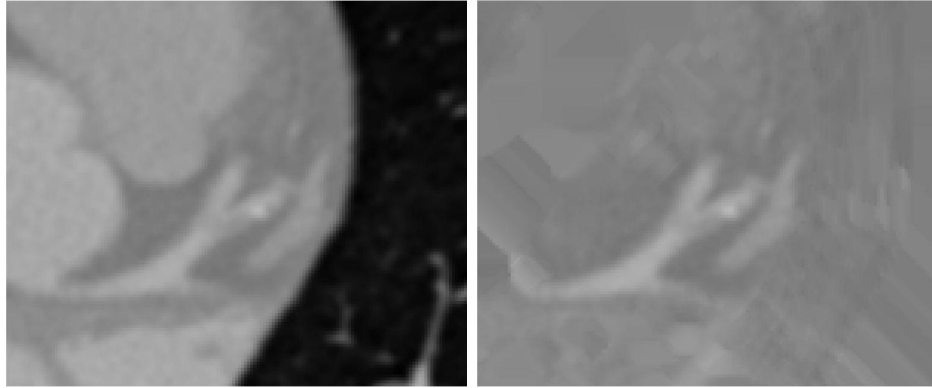


Figure 22: Dataset2: Before and After Blob and Lung Correction

driven active contour model segments the blood lumen from the cardiac muscle and the soft plaque. The segmented blood lumen is dilated considerably so that it will encompass the soft plaque deposits. The dilated surface is then subjected to the curvature flow in Equation 35. The average intensities of the cardiac muscle and soft plaque and that the cardiac muscle and blood were separable by using the Chan and Vese model as the local region based function. The segmentation method was tried on a 2D domain on slices of two different datasets and the results are given in Figures 23 to 25(for dataset1) and 26 to 28(for dataset2). The red contour shows the results of the Bayesian based vessel segmentation. The initial contour and final result of the hybrid scheme are shown as blue contours. The region between the red contour and the blue contour includes the soft plaque deposits.

Out of the 8 datasets for which the expert cardiac radiologist (Dr. Arthur Stillman

of Emory) had identified the location of the soft plaque, we chose 2 datasets where the soft plaque intensities were nicely homogeneous and that had no noise artifacts due to the presence of stents. We applied the blob/lung correction to fill the blobs and lungs with the intensity value of cardiac muscle. For the purpose of the local energy term for segmentation, we tried using the region based energy scheme proposed by Yezzi *et al.* [24] and the energy scheme proposed by Chan and Vese [26]. We got good results with the Chan and Vese scheme. The Yezzi based energy scheme did not work well because the scheme tries to minimize the energy by pulling the mean intensities inside and outside the local region of the contour as far apart as possible. However, the mean intensities of the blood, plaque and cardiac muscle near the edges are close to each other. Moreover, the curve evolution equation has an extra Area term in the denominator and is not suitable because the neighborhood that was chosen is small.

The results of the soft plaque segmentation by the hybrid scheme (based on Chan-Vese model) in 3D for the 2 datasets are shown in Figure 29 and 30. The evolution was done in 3D and the segmentation results for each slice is shown. For the dataset 1, the soft plaques were identified in slices 7 to 14 (order of slices: Left to Right and Top to Bottom) in Figure 29. For dataset 2, the method identifies the soft plaque in slices 1 to 2 and 4 to 5 in Figure 30. The results were compared against the ground truth provided by expert radiologists and our method was able to automatically identify the plaque. However, the ground truth provided by the radiologists did not have the exact segmentation of the plaque. Hence we were not able to quantify the comparison between our segmentation and the ground truth. This method was able to identify and provide a good segmentation of the soft plaque even when the plaque was smaller in volume (dataset 2).

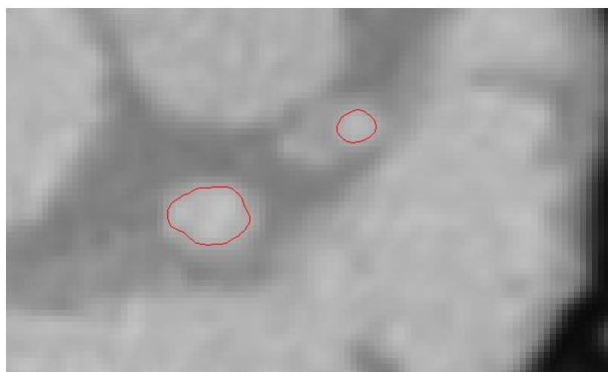


Figure 23: Dataset1: A 2D Slice of the dataset

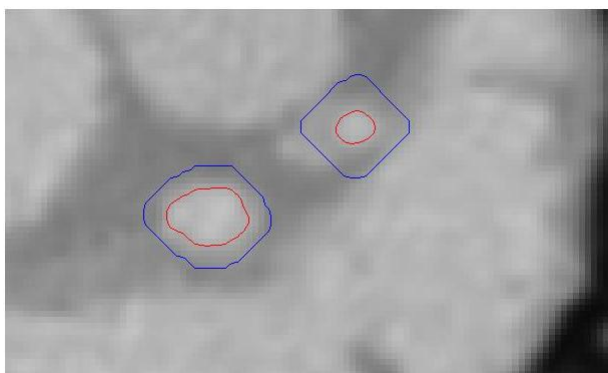


Figure 24: Dataset1: Initial Contour for Hybrid scheme

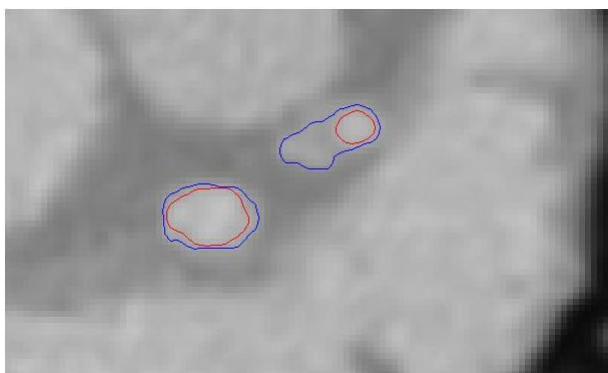


Figure 25: Dataset1: Final Contour after evolution

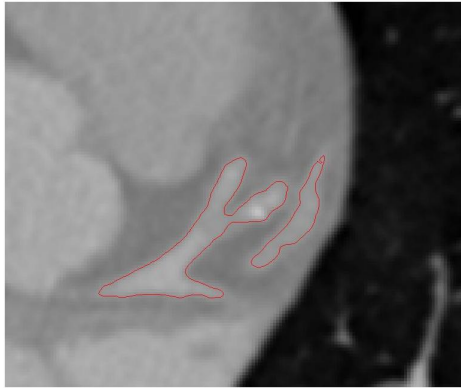


Figure 26: Dataset2: A 2D Slice of the dataset

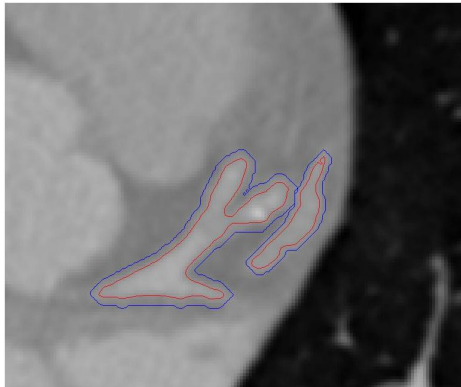


Figure 27: Dataset2: Initial Contour for Hybrid scheme

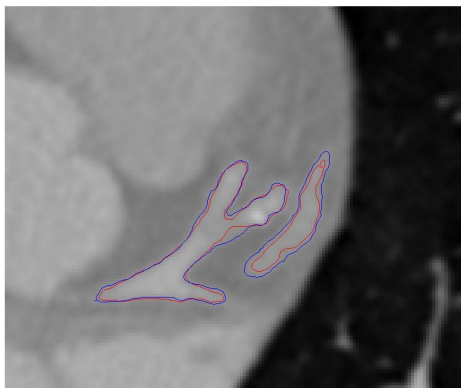


Figure 28: Dataset2: Final Contour after evolution

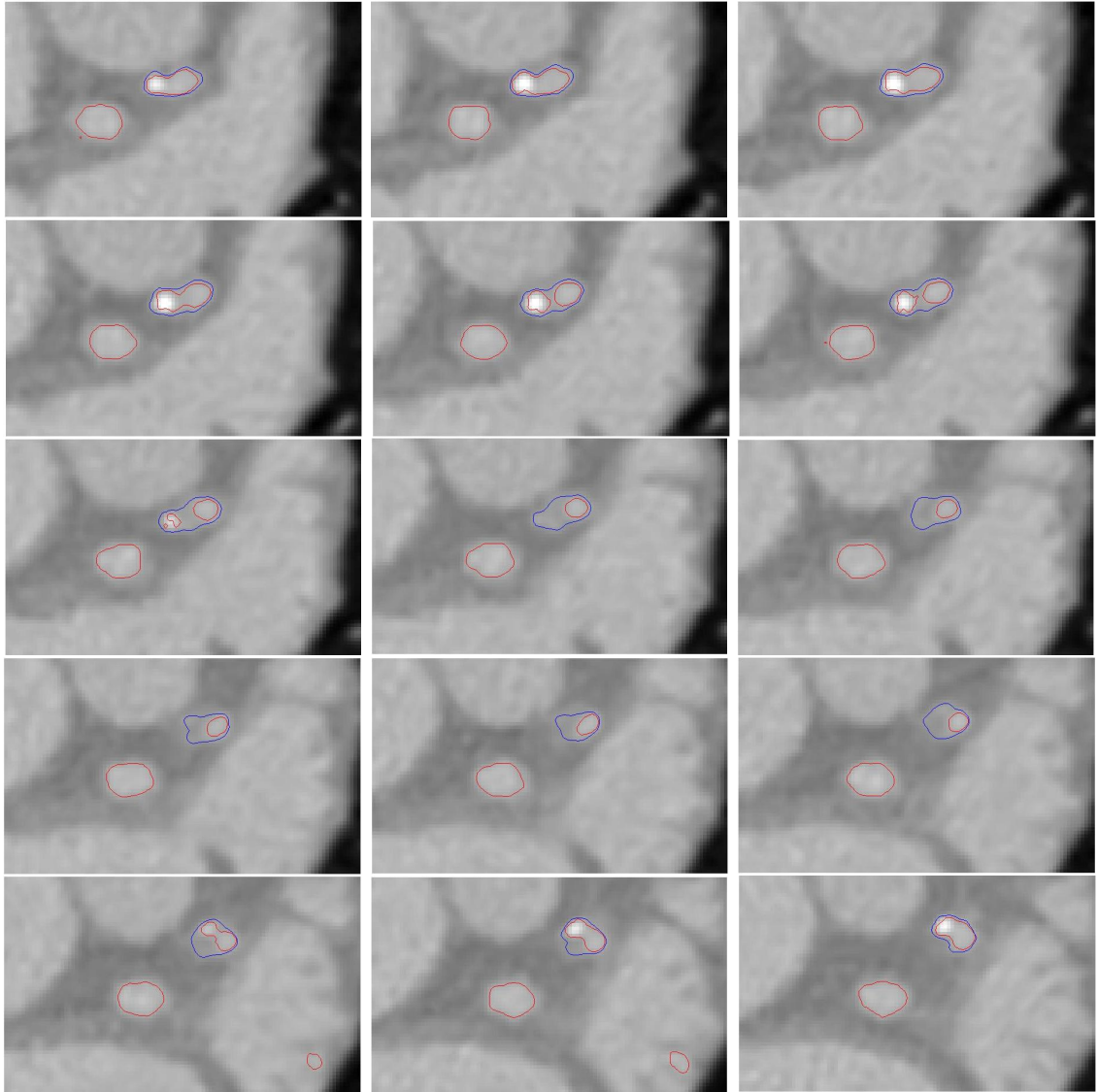


Figure 29: Dataset1: Result of 3D Segmentation using Local Region based energy.

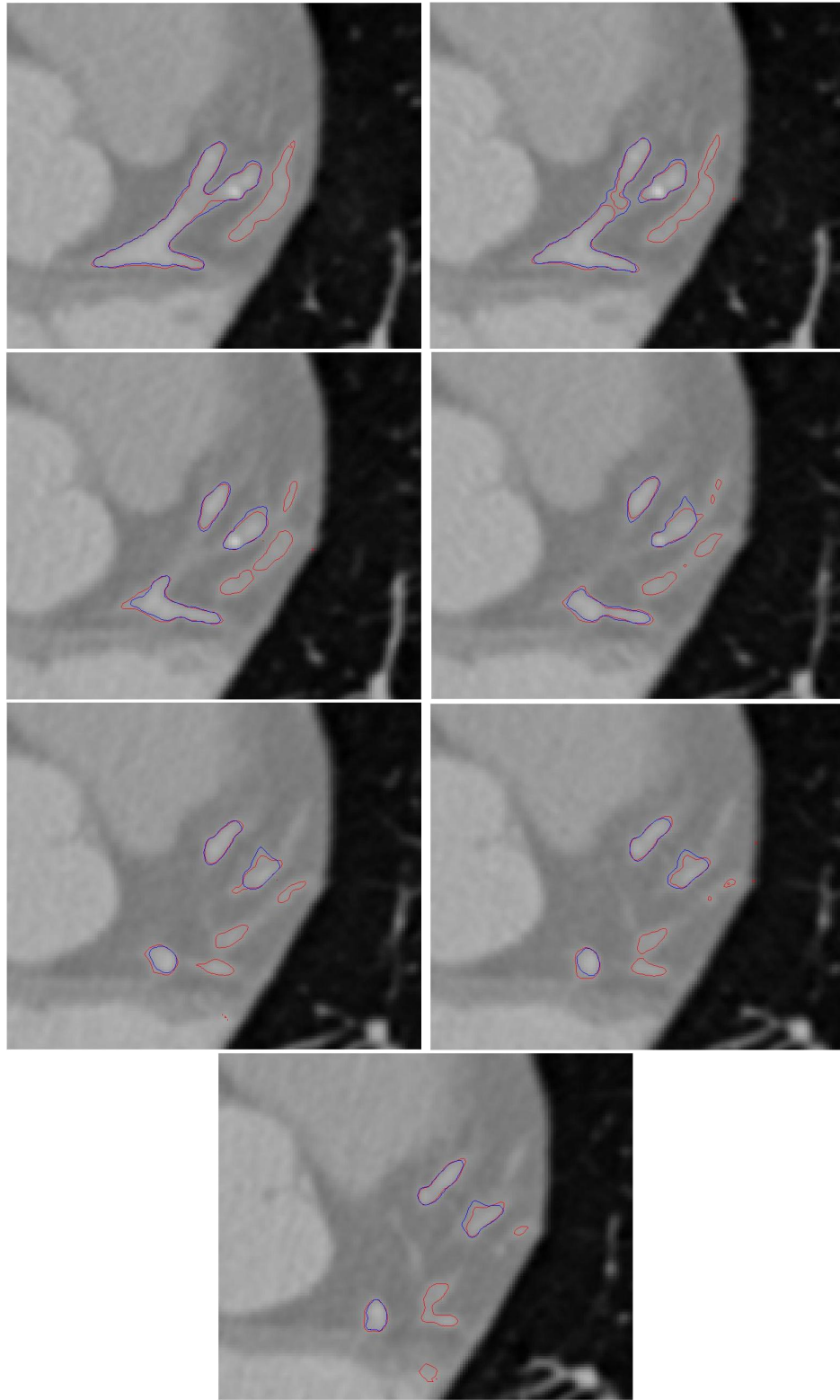


Figure 30: Dataset2: Result of 3D Segmentation using Local Region based energy.

CHAPTER V

CONCLUSION

In this thesis, we described two possible schemes that may be used to detect and segment the soft plaque present in the coronary arteries. In the first method, we used the structural changes induced by the plaque deposit to identify the location of the plaque. This method works well in the identification of larger plaques and does not provide an accurate segmentation of the plaque.

We proposed a second approach that is based on a novel hybrid active contour scheme and can be used to identify smaller plaques and provide an actual segmentation of the plaque. This technique has a great deal of potential for providing accurate segmentation of soft plaque which can be used for the characterization of the soft plaque deposit. In the future, this method should be applied to many more datasets for which the ground truth segmentation is available and a quantitative study of the performance should be done. Innovative local region based energy functions based on the hybrid active contour framework can be researched extensively to make the segmentation more robust even when the data is noisy due to the presence of cardiac stents and imaging artifacts.

REFERENCES

- [1] Veronica Rolim S. Fernandes *et al*, Atherosclerosis imaging and heart failure, Heart failure reviews, Volume 11, Number 4 / December, 2006, 279-288
- [2] Russell Ross, Atherosclerosis—An inflammatory disease, The New England Journal of Medicine, Jan 14, 1999, Vol 340, Issue 2; 115-127
- [3] R A Coulden *et al*, High resolution magnetic resonance imaging of atherosclerosis and the response to balloon angioplasty, Heart, Feb 2000; 83: 188-191.
- [4] Jeffrey M. Schussler and Paul A Grayburn, CT imaging of the coronary arteries, Heart, Dec 2005; doi:10.1136 hrt.2005.069195
- [5] Jerry L. Prince, Jonathan Links, “Medical Imaging Signals and Systems”, First edition (April 25, 2005), Prentice Hall.
- [6] <http://www.aurorahealthcare.org> and <http://www.nucleusinc.com>
- [7] <http://www.raymedical.com/technologie/CT.php>
- [8] <http://research.physics.lsa.umich.edu/chupp/Physics290/2003Lecture6.pdf>
- [9] Roger J. Webster, Convexity, Oxford University Press, 1994
- [10] Osher, S. and Fedkiw, R., *Level Set Methods and Dynamic Implicit Surfaces*, Springer-Verlag, 2003.
- [11] Sethian, J., “Level Set Methods and Fast Marching Methods”, *Cambridge University Press* (1999)
- [12] Sethian, J. A., “A review of recent numerical algorithms for hypersurfaces moving with curvature dependent speed,” *J. Differential Geometry*, vol. 31, pp. 131-161, 1989.
- [13] Yang, Y., Tannenbaum, A., and Giddens, D., “Knowledge-Based 3D Segmentation and Reconstruction of Coronary Arteries Using CT Images”, *In Proceedings of the 26th Annual International Conference of the IEEE EMBS*, (2004) pp. 1664-1666.
- [14] Yang, Y., Zhu, L., Haker, S., Tannenbaum, A., and Giddens, D. P., “Harmonic Skeleton Guided Evaluation of Stenoses in Human Coronary Arteries”, *MICCAI 2005, LNCS 3749*, (2005) pp. 490-497.
- [15] Frangi, A. F., Niessen, W. J., Vincken, K. L. and Viergever, M. A., “Multi-scale Vessel Enhancement Filtering”, *MICCAI’98, LNCS 1496*, (1998) pp. 130-137

- [16] Kichenassamy, S., Kumar, A., Olver, P., Tannenbaum, A., and Yezzi, A., “Conformal Curvature Flows: From Phase Transitions to Active Vision,” *Archive of Rational Mechanics and Analysis*, **134** (1996) pp. 275-301.
- [17] Olver, P., Sapiro, G. and Tannenbaum, A., “Invariant Geometric Evolutions of Surfaces and Volumetric Smoothing”, *SIAM J. Applied Math.*, 57 (1997) pp. 176-194.
- [18] http://www.mathworks.com/company/newsletters/news_notes/win02/watershed.html
- [19] Caselles, V., Kimmel, R., and Sapiro, G., “Geodesic Active Contours,” *Int. Journal Computer Vision*, **22(1)** (1997) pp. 61-79.
- [20] D. Adalsteinsson and J.A. Sethian, “A Fast Level Set Method for Propagating Interfaces *Journal of Computational Physics*”, Vol. 118, pp. 269-277, 1995.
- [21] S. Beucher, “Watersheds of functions and picture segmentation” , *Proc. IEEE int.. conf. Acoustics, Speech and Signal Processing, 1928-1931, 1982*
- [22] Vincent and Luc and Pierre Soille, “Watersheds in Digital Spaces: An Efficient Algorithm Based on Immersion Simulations”, *IEEE Transactions of Pattern Analysis and Machine Intelligence*, 13(6), 583-598, 1991
- [23] S. Lankton, D. Nain, A. Yezzi, and A. Tannenbaum, “Hybrid Geodesic Region-Based Curve Evolutions for Image Segmentation”. In *SPIE Medical Imaging*, Vol. 6510, 2007
- [24] J. A. Yezzi, A. Tsai, and A. Willsky, “A fully global approach to image segmentation via coupled curve evolution equations,” *J. Vis. Comm. Image Rep.*, vol. 13, no. 1, pp. 195–216, Mar. 2002.
- [25] D. Mumford, “A bayesian rationale for energy functionals”, In *Geometry Driven Diffusion in Computer Vision*, B. Romeny, ed., Kluwer Academic, Dordrecht, pp. 141.153, 1994.
- [26] T. Chan and L. Vese, “Active contours without edges”, *IEEE Trans. on Image Processing* 10(2), pp. 266.277, 2001.
- [27] M. Kass, A. W. and Terzopoulos, D., “Snakes: active contour models,” *Int. Journal of Computer Vision*, vol. 1, pp. 321-331, 1987.
- [28] Yuille, A., Cohen, D., and Halliman, P., “Feature extraction from faces using deformable templates,” in *Proc. CVPR*, pp. 104-109, IEEE, 1989.
- [29] Y. Rathi, O. Michailovich, J. Malcolm, and A. Tannenbaum, “Seeing the unseen: Segmenting with distributions,” *Proc. Int. Conf. Sig. Imag. Proc.*, 2006
- [30] T. Kailath, “The Divergence and Bhattacharyya Distance Measures in Signal Selection,” *IEEE Trans. on Comm. Technology*, vol. 15, pp. 52-60, Feb. 1967.

- [31] Goudail, F., Refregier, P., Delyon, G., “Bhattacharyya distance as a contrast parameter for statistical processing of noisy optical images”, *Journal of Optical Society of America* 21 (2004)
- [32] Dempster, A., Laird, N., and Rubin, D., “Maximum Likelihood From Incomplete Data Via the EM Algorithm”, *Journal of the Royal Statistical Society, Series B*, 39(1), (1977) pp. 1-38
- [33] McLachlan, G. and Krishnan, T., “The EM Algorithm and Extensions”, Wiley series in probability and statistics, John Wiley & Sons.
- [34] Gonzalez and Woods, “ Digital Image Processing”, 3rd Edition, Prentice Hall
- [35] Sethian, J.A., “A Fast Marching Level Set Method for Monotonically Advancing Fronts”, *Proceedings of National Academy of Sciences*, 93, 4, 1996.
- [36] Kimmel, R. and Sethian, J.A., “Computing Geodesic Paths on Manifolds”, *Proceedings of National Academy of Sciences, USA*, 95(15): 8431-8435, 1998.